Science Arts & Métiers (SAM)

is an open access repository that collects the work of Arts et Métiers Institute of Technology researchers and makes it freely available over the web where possible.

This is an author-deposited version published in: https://sam.ensam.eu
Handle ID: .http://hdl.handle.net/10985/9667

To cite this version :

Maxence BIGERELLE, Jean-Marie NIANGA, Alain IOST - Decomposition of a tribological system by chaos theory on rough surfaces - Tribology International - Vol. 82, p.561-576 - 2015

Any correspondence concerning this service should be sent to the repository Administrator : scienceouverte@ensam.eu

Arts et Métiers Institute of Technology

Decomposition of a tribological system by chaos theory on rough surfaces

M. Bigerelle [a,*], J.M. Nianga [b], A. Iost [c]

[a] Laboratoire TemPo/LAMIH UMR8201, Université de Valenciennes, Le Mont Houy, 59313 Valenciennes, France
[b] Equipe Mécanique des Structures, Hautes Etudes d'Ingénieur, 13 Rue de Toul, 59046 Lille Cedex, France
[c] Arts & Metiers ParisTech; Mechanics, Surfaces and Materials Processing (MSMP), 8, boulevard Louis XIV, 59046 Lille, France

Keywords:
Tool machining
Chaos theory
Roughness
Machinability

A B S T R A C T

The purpose of this paper is to analyze the turning machinability of a martensitic steel, according to the cutting speed, and through signal analyses of the morphology of the machined surface. We initially carried out the classification of a large number of parameters of roughness, on the basis of their relevance with regard to cutting speed. The originality of the proposed method lies in the combination of the classical technique of analysis of variance with the statistical technique of resampling of data, called Bootstrap. Another characteristic of the study consists in the addition to the traditional categories of roughness parameters (Amplitude, Frequency, Morphological and Hybrid parameters) to analyze multi-scale aspect of surface topography through fractal analysis. According to the analysis carried out, the fractal dimension and the slope of the signal (dz/dx) of the topographical signal of the studied surface appear much more relevant than all the other Euclidian parameters. The fractal dimension and the slope of profile allow us to estimate a critical transition speed between the cutting states by generalized strain hardening and those by localized strain hardening. This parameter is also more relevant than the others, because it allows a good analysis of the influence of cutting speed, within each of the two machining modes. The obtained result is relevant because it provides a practical and inexpensive method for the quality control of the machined surface, to manufacturers and engineering companies, without removing some mechanical part, but only through a direct analysis of the slopes of the profile, with, in particular, the help of a portable instrument. We establish later that the transition between disorder and order of the aspect of the observed profiles is essentially due to an instability, which we analyze by the chaos theory. For that purpose, we propose an original construction of an attractor that presents a fixed point for low cutting speeds. This attractor characterizes, beyond the critical cutting speed, an instability described by a phenomenon of successions of states on the attractor between work hardening by localized shear plastic deformation and softening due to the rise in temperature.

1. Introduction

The improvement of the processes of quantification of the state of machined surfaces is always one of the major concerns for many researchers and industrialists. However, quality control of these surfaces generally requires an analysis of their roughness (signal of the surface), whose choice of parameters has often been the object of many controversies because of multiple possibilities of collection and interpretation of data, in general related to statistical analysis, and in particular to roughness profiles (roughness signal). We point out that certain parameters of roughness usually used, such as the average deviation of roughness R_a (*arithmetic mean of all the ordinates of the profile over a basic length),* have appeared in the international standards *(ISO 4287*) only since roughly fifteen years. Previously, each country had its own parameters, and in addition, had its own methods of calculation. The question of choosing the most relevant parameter of roughness thus remains particularly delicate, especially if we take into account the conditions of measure as well as the characteristics of the measuring device. Thus in this study, we consider the various evolutions in the relation between the tool, the matter and the process, in order to ensure an optimal use of the machined surfaces, as well as possible productivity gains. We thereafter use the chaos theory to explain the transition between generalized strain hardening and localized strain hardening. This transition is, in particular, described through the analysis of the evolution of the average

* Corresponding author. Tel.: +33 616 297 604.
E-mail address: maxence.bigerelle@utc.fr (M. Bigerelle).

Nomenclature

$\overrightarrow{A}_i$	vector of physical parameters in the space phase i
$B(x)$	Uniform noise in the range 0 and 1
D	Euclidian dimension of the space phase
$M_1, M_2, \ldots, M_D$	mechanisms creating the space phase
R_a	mean of signal amplitude $R_a = 1/L\int_L \lvert z(x)\rvert dx$
R_t	range of signal amplitude
T	cutting temperature
$U(x)$	Modeled signal of tooled surface
V_c	cutting speed
x	scanning length of signal roughness
$z(x)$	signal amplitude of the surface
β	a factor lying between 0 and 100
Δ_a	mean slope of profile $\Delta_a = (1/L)\int_L \lvert \partial z(x)/dx\rvert dx$
$\partial\tau/\partial\gamma$	strain hardening
γ	shear strain
τ	shear stress

slope of the estimated profiles (dz/dx, where z is the amplitude of the topography and x the sampling length of the surface). Two types of behavior are likely to cause a change in the machined surface: chatter and machinability. Whereas the first concerns primarily the vibratory aspect of the tool, appearing, except in the event of instability, through a topography of the machined surface with relatively periodic patterns, the second is dependent on the stakes of balance between strain hardening, which tends to harden the material, and thermal softening, due to the heat that is released at the cutting time. A localized shear plastic deformation will thus tend to support the machinability of the surface, while a prevalence of strain hardening would block it. The cutting process is then carried out through a wrenching of material. The instability of the structure observed for high speeds that we propose to model by the means of the chaos theory would thus be explained by the alternation of a strain hardening state and a thermal softening of material. The studied surfaces come from a stainless steel martensite of type Z210CW12. The tests were carried out under the following conditions:

- cutting speeds V_C in m min^{-1} ($65 \leq V_C \leq 200$),
- feed rate: 0.15 mm tr^{-1} and
- cutting depth: 0.5 mm.

The measurement of surface roughness is carried out perpendicularly to the machining grooves using a mechanical profilometer (KLA Tencor P10™) with an evaluation length of 15 mm and a sampling length of 0.4 μm.

The paper is organized as follows: in Section 2, the method of statistical treatment used to analyze the relevance of conventional roughness parameters is presented. Section 3 is devoted to the results of this conventional analysis of roughness. In Section 4, we analyzed the topography via the chaos theory. Section 5 deals with the results' interpretation of the machinability analysis via the same highlighted theory.

2. The conventional analysis of roughness

The studied surfaces are machined at the 10 following cutting speeds: 65, 80, 95, 110, 125, 140, 155, 170, 185 and 200 m/min. For each of these 10 samples, 30 profiles are implemented by means of the software Mesrug™ that is conceived by our research teams [1,2]. Besides, for each of the profiles, 95 roughness parameters are measured and distributed according to 10 classes (Fig. 1) containing amplitude parameters (R_a, R_t,…), frequency parameters (*number of peaks, spectral moments, length of autocorrelation*), hybrid parameters (*slopes of the profiles, area ratio of surface*), and parameters resulting from the fractal analysis (*fractal dimension, slope of the spectral density*).

However, for the determination of the most relevant parameters, we propose in this paper an original technique of variance analysis: *ANOVA by bootstrap* [3,4]. This technique is of such great importance that the statistical approach used in this study requires a large number of parameters. Besides, similar to the classic *ANOVA*, this technique allows the determination of the parameter containing maximum information on a given class. It allows later an estimation of the influence of this class, through the definition of a Fischer variable F, as well as of a critical probability below which we could wrongly assert the aforementioned influence. However, unlike the traditional *ANOVA*, the variable F is considered as a random variable according to *ANOVA by bootstrap*. This random behavior is essentially due to data variation which, besides, implies a variation of the critical probability. Let us note too that the more the value observed by the variable F corresponding to a given cutting parameter is large, the more this last one will be considered as a discriminant parameter according to the cutting speed (Fig. 2).

3. Results of the conventional analysis of roughness

According to the conventional analysis described in the previous paragraph, the three most relevant parameters (Table 1) were examined:

Although the average deviation of roughness R_a is one of the roughness parameters that is most usually used in the traditional analysis of machined surfaces, it is not, in this study, the most relevant parameter for the characterization of cutting speed effect on machinability. In order to illustrate these results, Figs. 3 and 4 present the comparison of the histograms of the Fischer variable for the three selected parameters, as well as the comparative studies of the box-plot for these last ones, according to cutting speed. These results are also confirmed on the basis of 8000 discretization points obtained using a portable profilometer Perthometer™ M4Pi, with a probe tip radius of 5 μm. One of the major consequences of this study is the possibility of quantifying the machinability in situ without taking off the machined part from the tool machine (Table 1).

3.1. Analysis of the relevance of parameter Δ_a

Mathematically, the mean value Δ_a of the profile slopes over a profile evaluation length L is described by a numerical function z, generally unknown, and defined by

$$\Delta_a = \frac{1}{L}\int_L \left|\frac{\partial z(x)}{\partial x}\right| dx \tag{1}$$

- The experimental results analysis shows a great decrease of the profile slopes Δ_a around a critical cutting speed V_C of 125 m/min. Indeed, for speeds lower than V_C, the profile presents a disordered aspect, whereas beyond this value a periodic component with weak noise appears. However, it is

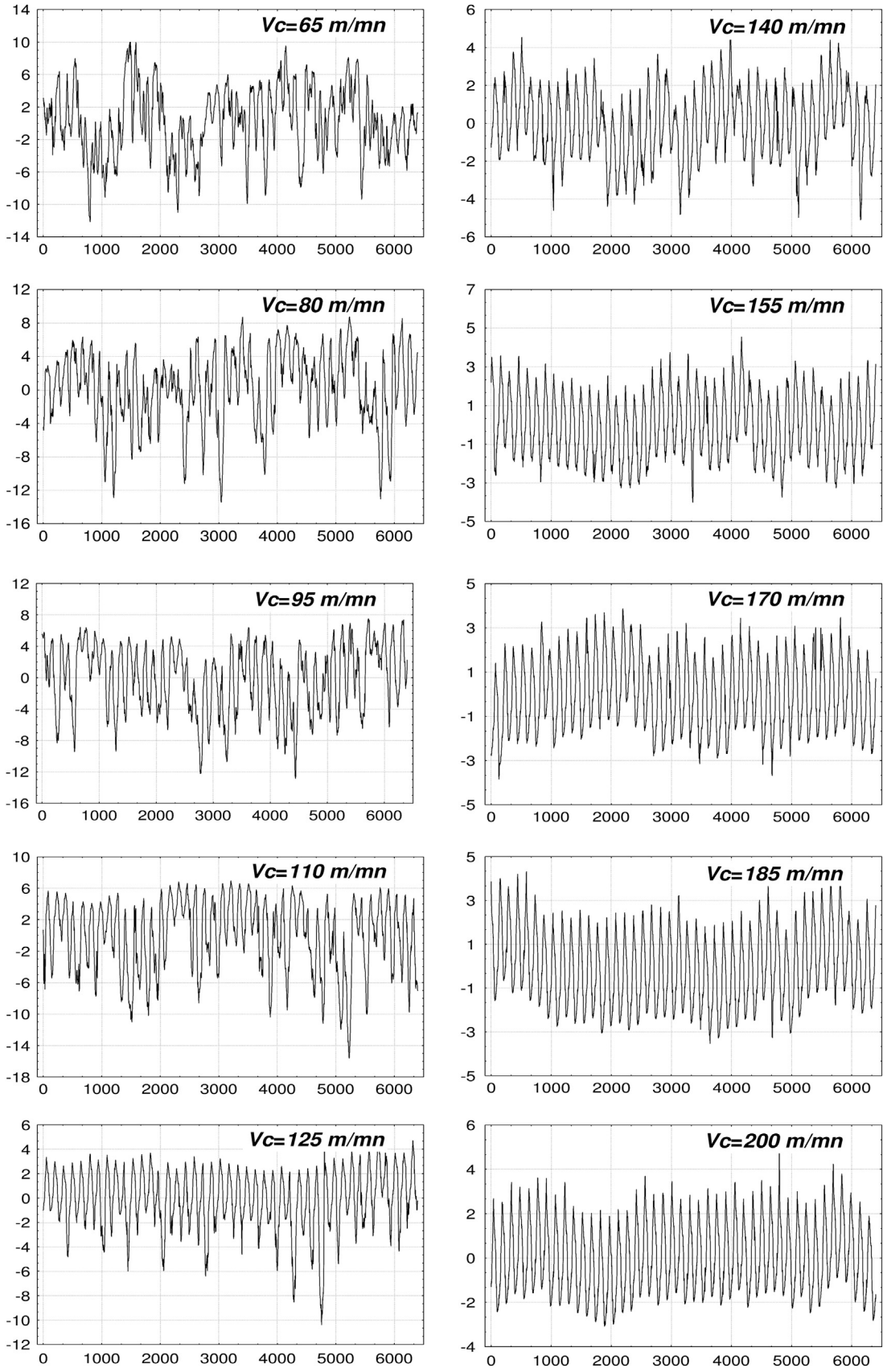

Fig. 1. Roughness profiles of tooled surfaces produced by turning process with different cutting speeds (in m/mn).

difficult to quantify the effect of a noise on the value of the slopes of the profile on experimental profile. To quantify this effect of parasite noise, a numerical simulation is performed:

A *T* profile is created using a half-cycle sinusoid that represents the modeling of the un-noised experimental profile. Then a uniform white noise *N* bounded in the [0..0.1] amplitude is

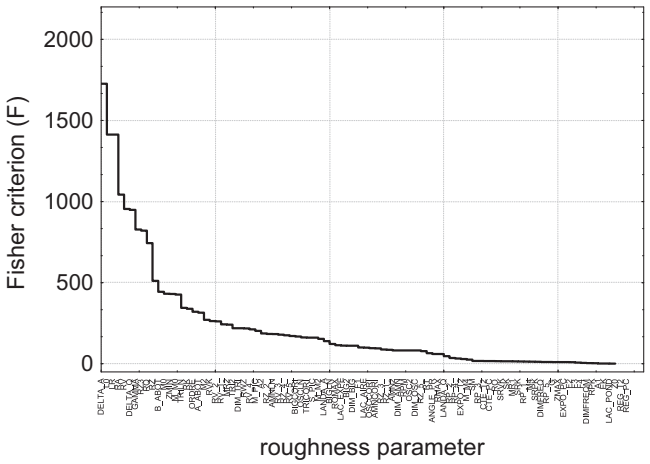

Fig. 2. F Fisher variate evolution versus roughness parameters.

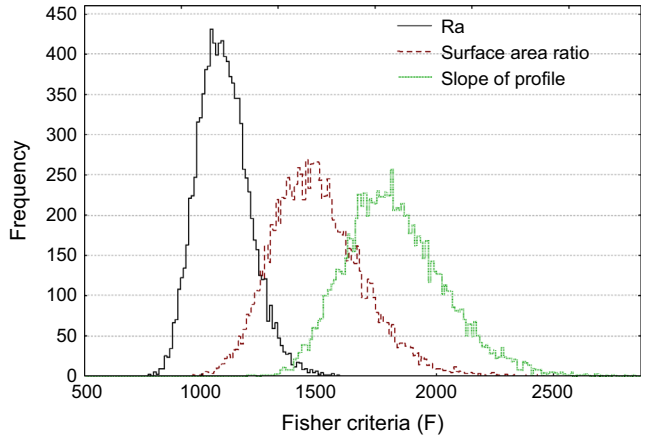

Fig. 3. F Histogram of Fisher values for the three more relevant roughness parameters: the mean slopes value, the developed area and the arithmetic roughness.

added to the T profile with an amplitude characterized by a coefficient β with $0 \le \beta \le 100$

$$z(x) = \frac{R_t}{50}[\beta T(x) + (100-\beta)(N(x)-0.5)], \quad (2)$$

When $\beta = 100$, simulated "tooled" surfaces are assumed to be machined without noise.

When $\beta = 0$, simulated "tooled" surfaces are reduced to a white noise.

The analysis of the Δ_a evolution curve according to the β factor (Fig. 5) reveals a decrease of the mean value of the profile slopes with decrease in noise. As a consequence, the decrease in the experimental slope of the profile with the increase of cutting speed can be seen as a decrease of a noise on the topographical map.

3.2. The conventional analysis interpretation

Many previous studies confirm the parameter Δ_a relevance, like its discriminant behavior. Consequently, it seems important to establish why this parameter's experimental values increase, when the cutting speed decreases. Three explanations appear plausible:

(H1). The depth of the grooves observed during the turning process would depend on the cutting speed.

(H2). A decrease of the cutting speed involves the cutting process by generalized strain hardening, leading to an increase of cutting

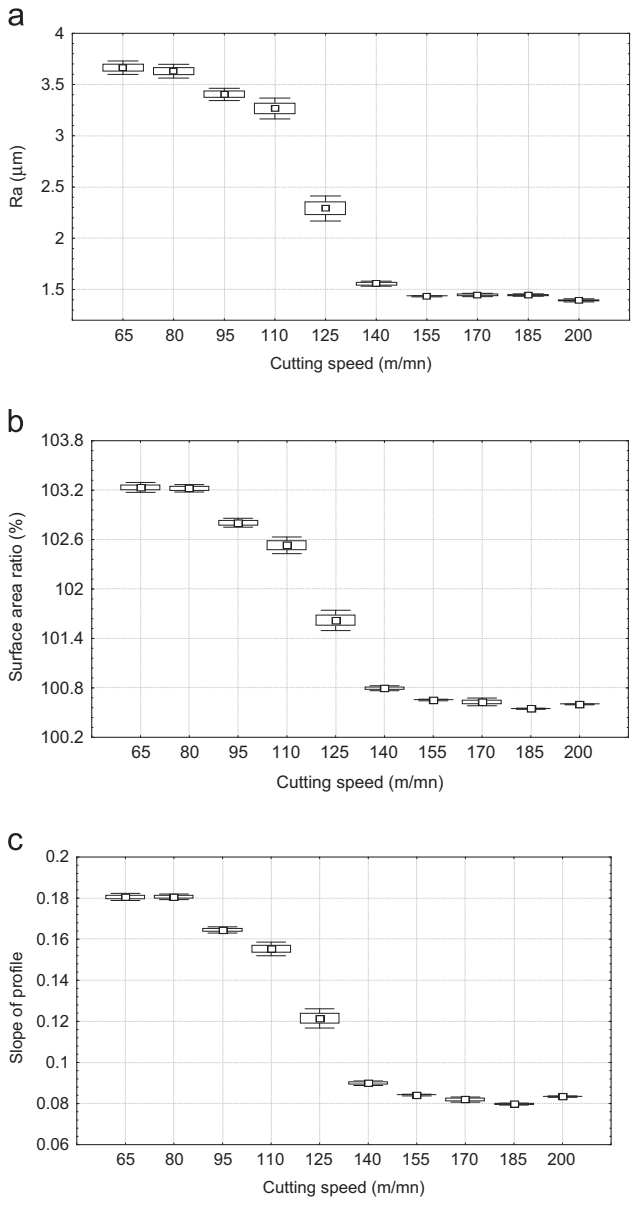

Fig. 4. Plot of the most pertinent parameters versus the cutting speed. (a) arithmetic roughness, (b) the developed area and (c) the mean slopes value.

Table 1
Fisher values for three more relevant parameters: the mean slopes value, the ratio of profile and the arithmetic roughness.

Selected parameter	Fischer variable observed average $\bar{f}$
Mean value of the slopes of the profile, D_a	1726
Ratio of profile, A	1413
Average deviation of roughness, R_a	1042

power. This increase could lead to a low-frequency machine tool vibration that would generate topographical waviness in the profile.

(H3). The generalized strain hardening corresponding to a cut carried out by plasticity would not allow a cut as regular as that obtained by localized shear deformation. As a consequence, generalized strain hardening would involve more important

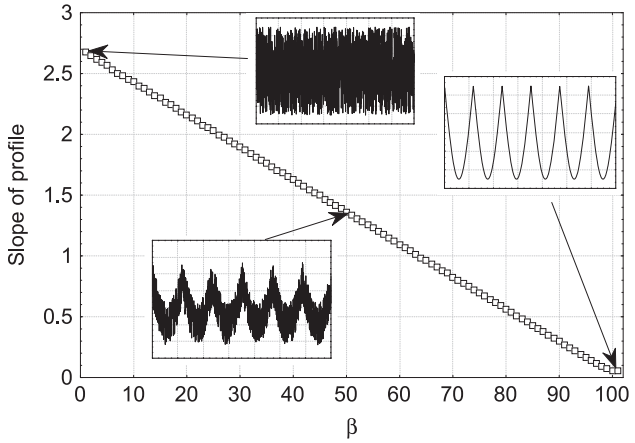

Fig. 5. Plot of the mean slopes value calculated from simulated profiles with white noise ($B=0$) and without white noise ($B=100$).

fluctuations of the plasticized zone and a noise without a narrow frequential signature (pink noise) would then be present on the totality of the profile. This pink noise is characterized by a signal or process with a frequency spectrum such that the power spectral density (energy or power per Hz) is inversely proportional to the power frequency of the signal according to the power relationship $P(f) \propto 1/f^{\alpha}$ with $\alpha \in [1,2]$. These pink-like noises occur widely in nature and are a source of considerable interest in many fields. The noise with a broad range of α approximately corresponds to a wide range of non-equilibrium driven dynamical systems.

These attempts of explanation thus lead us to carry out a spectral analysis of the profile of the machined surface.

3.2.1. Interpretation of the spectral analysis for the machined surface profile

We have precisely carried out the calculation of the discrete Fourier transform for each of the 30 profiles obtained for each cutting speed, and thus have obtained the discretized spectrum $(f_i^{v_{c_j}} P(f_i^{v_{c_j}}))_{\left\{\begin{smallmatrix} i=1,2,n_j \\ j=1,2,..30 \end{smallmatrix}\right\}}$, where $P(f_i^{v_{c_j}})$ indicates the power spectral density carried by the frequency of order j for the profile obtained at speed v_{c_j}. The graphic representation of the spectrum in a bi-logarithmic coordinates system, for each cutting speed (Fig. 6b), presents a harmonic around 150 μm corresponding to the feed rate of $0.15_{\pm 0.2}$ mm/rev (Fig. 7). This value is independent of the cutting speed. The machining process thus allows a perfect control of the feed whatever the state of generalized strain hardening. However, as the variation of the maximum amplitude of the peak described above is weak, compared to that of the noise level observed, one could, at first approximation, regard it as a constant. As a consequence, cutting depth is constant and assumption (H1) can be rejected. This analysis suggests a formulation of the machinability in the form of a sum of two independent functions. The first of these is periodic function, depending on the tool shape, the feed rate and the feed depth, respectively. The other one is an aperiodic function which characterizes the machinability (pink noise). Analytically, when indicating by U, the machined profile representative function, and by B, the one which represents a unit pink noise which can be added to the signal and the profile $z(x)$

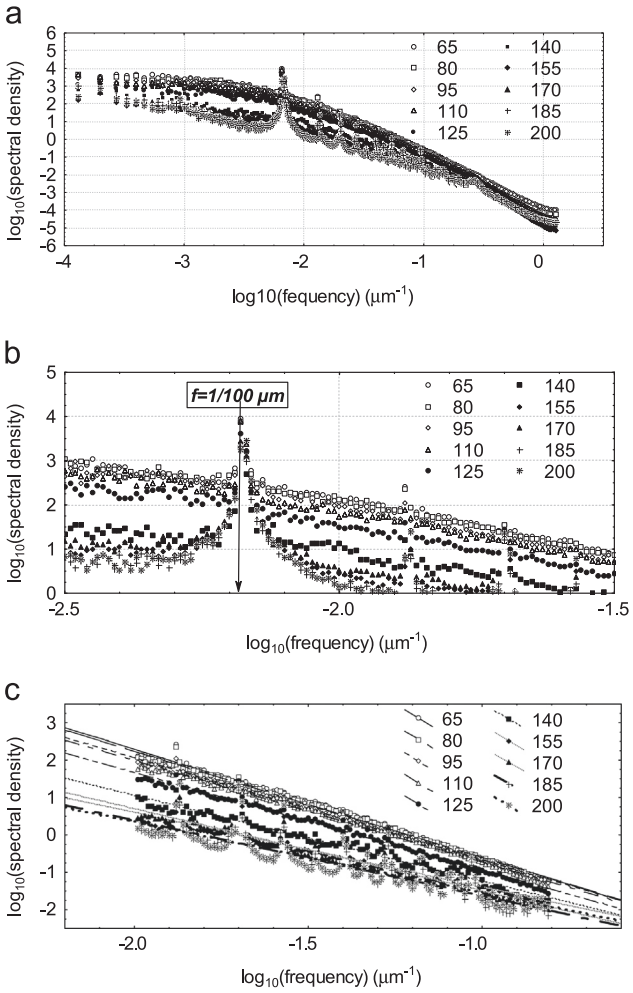

Fig. 6. (a) Power Spectrum density function of profiles shown on Fig. 1. (b) Zoom of power spectrum of (a) around the highest amplitude frequency. (c) Slope analysis of the power spectrum at varying cutting speeds.

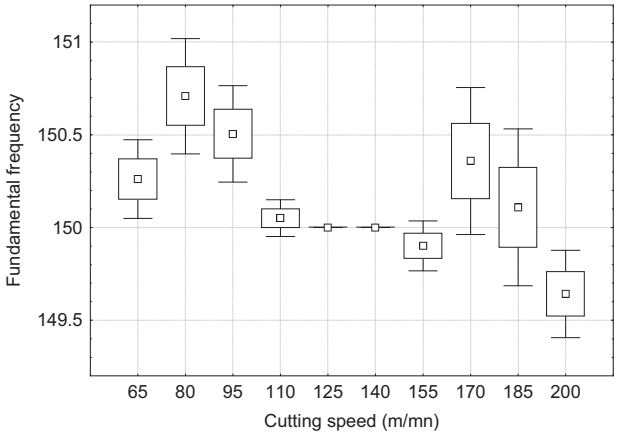

Fig. 7. Values of the wavelength of the highest amplitude frequency (Fig. 6b) at different cutting speeds.

can be modeled by

$$\begin{cases} z(x) = R_t U(x) + \beta B(x) \\ 0 \le B(x) \le 1; \quad 0 \le \beta \le 1 \end{cases} \tag{3}$$

Let us now introduce the discretized average spectrum, defined on all the 30 profiles corresponding to the same cutting speed b, as

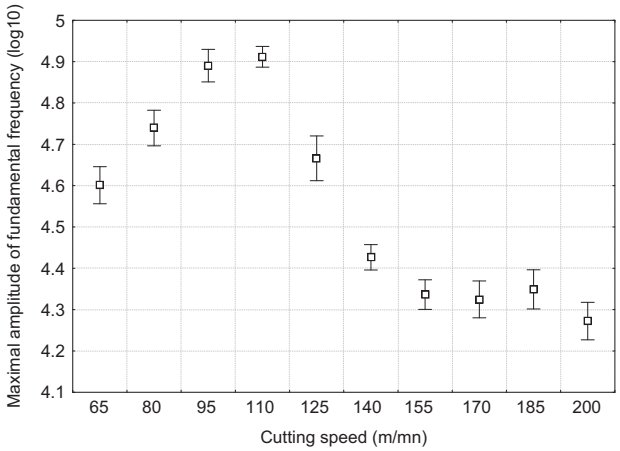

Fig. 8. Values of the highest amplitude of the power spectrum at different cutting speeds.

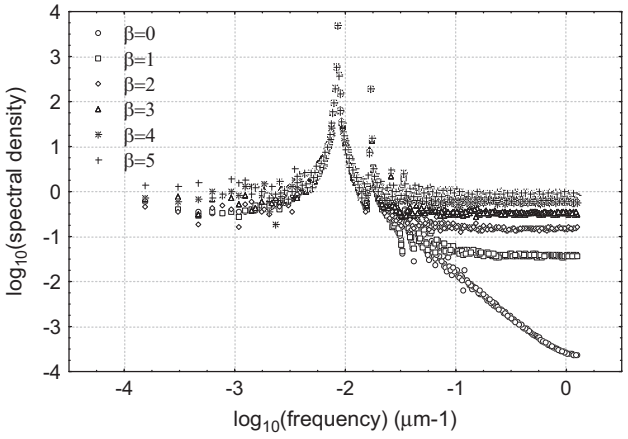

Fig. 9. Power spectrum of simulated profiles (in $\log_{10}$) versus frequency (in $\log_{10}$) by varying added unitary white noise $B(x)$ with $\beta \times B(x)$.

follows:

$$\left(\frac{1}{30}\sum_{j=1}^{30} f_i^{v_{C_j}}, \frac{1}{30}\sum_{j=1}^{30} P(f_i^{v_{C_j}})\right)_{\{i=1,2,n_j\}} \quad (4)$$

Under the conditions defined in [9], if the average spectrum verifies the power relationship $P(f) \propto 1/f^{\alpha}$, then the fractal dimension of the corresponding profile is then given by

$$\Delta = (5-\alpha)/2 \quad (5)$$

where α indicates the median value of the spectrum slope in the log–log plot. However, when $\beta = 0$ in Eq. (3) (half-sinusoidal profile), the α computation paradoxically provides 1.5 as fractal dimension rather than unity. This error which systematically appears, when evaluating the fractal dimension by the above relation, was analyzed by Brewer et al. [10]. On the other hand, as the analysis of the machined surfaces spectrum does not highlight any harmonic for low frequencies ($\log(f) < -2.5$), no cutting tool vibration will be at the origin of the growth of R_a for low cutting speeds. As a consequence, hypothesis (H2) is rejected and this R_a growth would thus be essentially explained by the presence of a characteristic pink noise introduced by the generalized strain hardening. In the following section, we then propose its fractal analysis (Figs. 8 and 9).

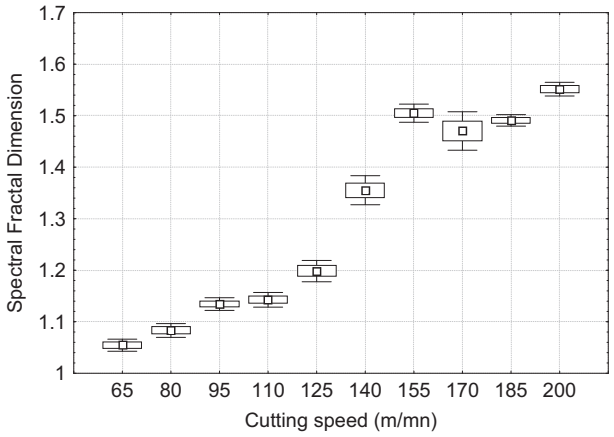

Fig. 10. Fractal dimension obtained from the power spectrum versus cutting speed.

3.2.2. *Fractal analysis of the machining noise*

The observation of the spectrum of Fig. 6 reveals 3 different modes:

- ***Decorrelation mode for the machining noise***: at low frequencies, the spectral power is constant meaning that no information exists.
- ***Fractal mode***: this mode corresponds to the spectrum evolution according to the power relationship $P(f) \propto 1/f^{\alpha}$. In this case, a study of the fractal dimension evolution reveals a Δ-quasi linear increase for the cutting speeds which are lower than 125 m/min (Fig. 10). The increase of cutting speed generates a heterogeneous distribution of the plastic zones, thereby increasing the heterogeneity of the generalized strain hardening. On the other hand, a regime change (high increase of fractal dimension) is observed after 125 m/min: the cut mechanisms pass from generalized strain hardening to shear plastic deformation, this latter being due to a localized strain hardening of the material. In this case, a chaotic alternation of hardening and softening appears that is characterized by a fractal dimension of 1.5. This fractal dimension appears as a particular Brownian process characteristic that we shall study in the following paragraphs, by means of the chaos theory.
- ***Euclidean mode***: this mode which corresponds to very high frequencies reveals the impact of smoothing effect on the change in spectra slopes. Note that this effect is due to the curvature radius of the tip radius of the profilometer. Therefore, the studied mode is simply related to a tactile measurement artifact.

4. Machinability analysis via the chaos theory

We have just established that the average slope of profiles is the most relevant parameter of roughness. It indeed highlights a transition between generalized strain hardening, which is characterized by low cutting speed and high profiles slopes, and localized strain hardening, characterized by high cutting speed and weak profiles slopes [11]. Consequently, the purpose of this study, in what follows, is thus to show that this transition is due to an instability which can be analyzed by the chaos theory. First, it is advisable to highlight the two types of behaviors which are involved in surface roughness modification.

4.1. *Origins of chaotic state*

The instabilities in the cutting process that change the surface topography can be due to 2 phenomena: machine tool chatter and machinability of materials.

a) ***Chatter:*** it originates in a vibratory aspect of the cutting machine, which involves a modification of the morphology of the surface, whose modeling requires solving two second-order differential equations of propagation type, and whose coupling is likely to involve an instability which characterizes the chaos [12–14]. On the other hand, the system tool-matter is characterized by a system mass-spring, implying a modeling in the elastic range. We thus postulate that chattering is a purely oscillatory phenomenon, which involves a disturbance of the morphology of surface on scales definitely more important than those corresponding to the interaction tool-matter.

b) ***Machinability***: the term machinability refers to the ease with which a metal can be machined to an acceptable surface finish. It is characterized by a transitory behavior resulting from the confrontation between the phenomena of strain hardening and thermal softening. Indeed, a surface will be machined much better under localized shear plastic deformation cutting. On the other hand, it will become weakly machinable if strain hardening is prevalent. The transition then occurs when the strain hardening effects are balanced by the thermal softening ones.

As regards the characterization of the tool-material coupling by the chaos theory, the general principle of approach which is suggested in this paper is as follows: for generalized strain hardening, the strain hardening mechanism is the only major phenomenon. Nevertheless, for localized shear plastic deformation, we postulate an alternation, for high cutting speeds, between the softening mechanism due to the heat released during the cutting process and the strain hardening phenomenon which tends to harden the material.

4.2. The mathematical problem of machinability by the chaos theory

We start with a short introduction to the chaos theory, and in particular, with a presentation of the famous Henon's attractor.

4.2.1. Introduction to the Henon attractor

The French astronomer Henon (1976) deducted a two-dimensional attractor from a three-dimensional Lorenz attractor, by considering the intersection of a fluid subjected to natural convection, with a transverse section in the flow direction [15,16]. The corresponding discrete time system is defined as follows:

$$\begin{cases} x(t+1) = y(t) + 1 - a[x(t)]^2 \\ y(t+1) = bx(t) \\ a = 1.4; b = 0.3 \end{cases} \quad (6)$$

The attractor graph (x, y) allows a multi-fractal structure which means that the fluid distribution in the space is not uniform (Fig. 11). It is then possible to obtain a graphic representation of the frequency at which an attractor point can belong to a fixed size cell. For that, after carrying out a discretization of the zone containing the attractor, through a mesh of size 1000×1000, we simulated 108 iterations. Fig. 11(b) represents, indeed, the probability density function of the presence within the phase's space of the attractor for which a simple observation allows the description of the subjacent multi-fractal structure. In the same way, it can be interesting to study the attractor behavior according to the parameter a of Eq. (6). For that, we build the *Feigenbaum* diagram (Fig. 12), which represents its state evolution $x(t)$, according to the parameter a. Then successive divisions called bifurcation appear due to chaos emergence. However, because the attractor is not known in our study, we will carry out its approximate rebuilding using the so-called delays method [17], on the basis of the only series of measures carried out on the cutting profile.

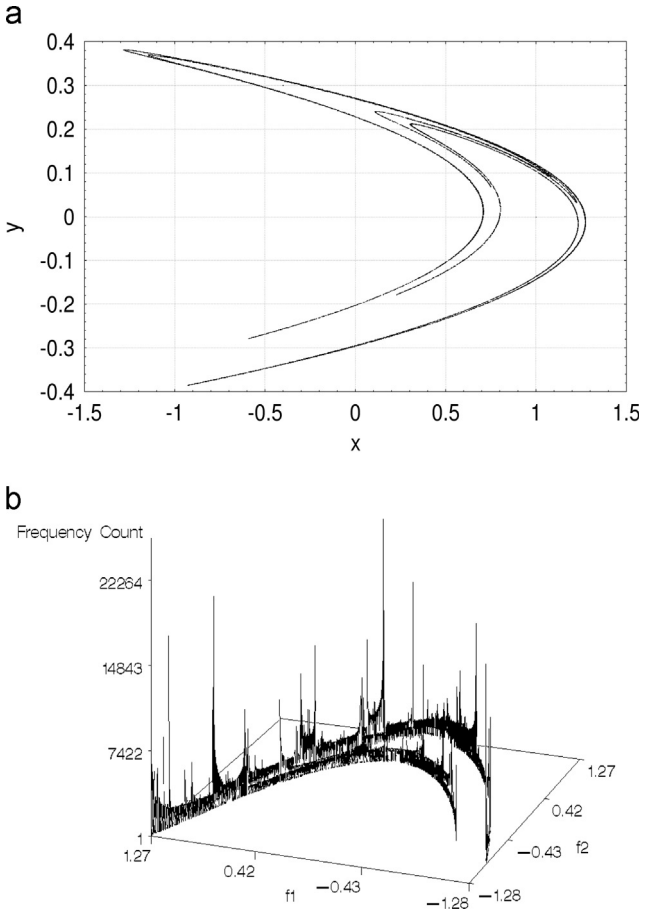

Fig. 11. Henon's Attractor in the x–y plane (a) and the empirical density probability function of the presence of (x, y) points.

4.2.2. Attractor rebuilding method

From the quantity $y(n)$ that represents the amplitude of the nth profile point, one can introduce, on the basis of a translation of the variable n, a so-called *delays vector*, which allows obtaining an attractor approximation, defined as follows:

$$z(n) = (y(n), y(n+k\tau), y(n+2k\tau), \ldots, y(n+(D-1)k\tau)) \quad (7)$$

where τ is the implemented sampling step and k is a number to be determined, representing a characteristic length. $y(n)$ represents, indeed, a pseudo-phase of the evolution of a state towards another. According to the delays theorem, $z(n)$ constitutes an attractor point. The rebuilding problem then consists, through a method allowing a visualization of the attractor projections, of determining the length k as well as the dimension D, beyond which the collected information does not result in any more precision. The application of this method to the Henon attractor leads to $D = 2$, which means that the representation of vectors $z(n) = (y(n), y(n+1))$ constitutes sufficient information for an attractor rebuilding (Fig. 13).

4.2.3. Attractor characterization for the machined surface profile

The creation mechanisms of the machined surface are supposed to be unknown and denoted by $M_1, M_2, \ldots, M_D$. They depend on variables $x_1, x_2, \ldots, x_D$, defined in a phases space (a phase space is a space in which all possible states of a system are represented, with each possible state of the system corresponding to one unique point in the phase space). On the other hand, the studied system M can then be expressed in the following form:

$$\partial x_i(t)/\partial t = M_i(A_i, x_1(t), x_2(t), \ldots, x_D(t)) \quad (8)$$

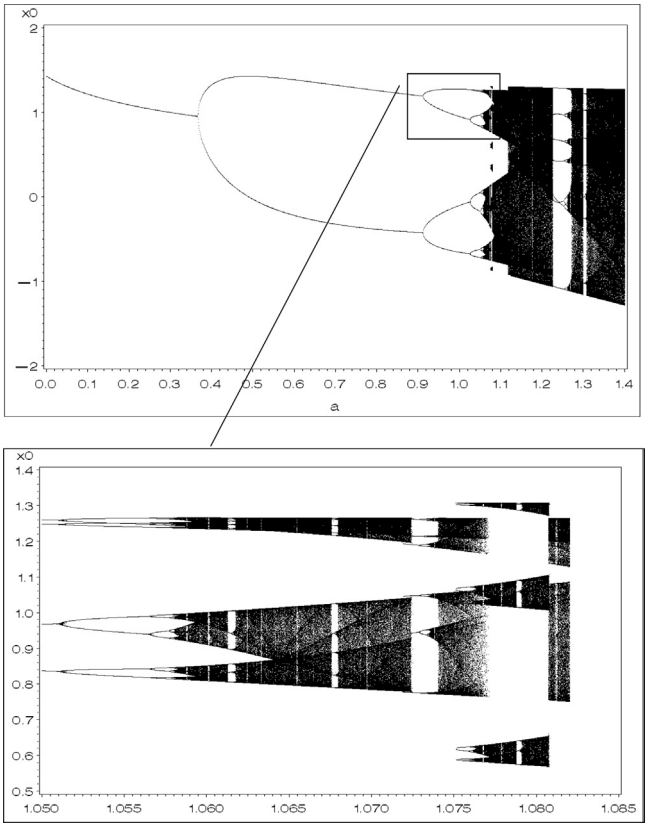

Fig. 12. Feigenbaum's plot of Henon's Attractor versus the parameter.

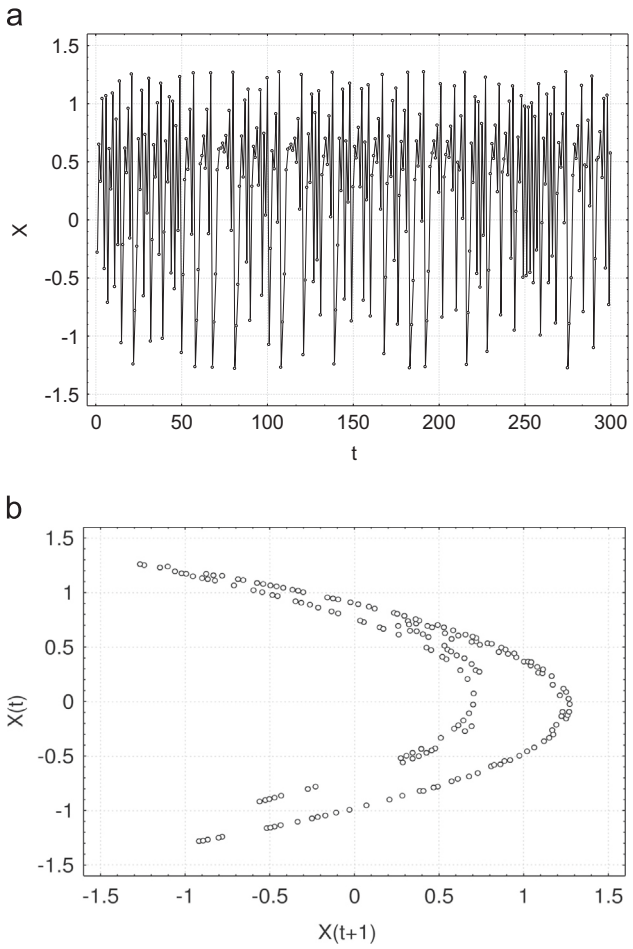

Fig. 13. Temporal plot of the x coordinate of Henon's Attractor versus the time t (a) and its reconstruction by the delay method (b).

where A_i is a vector of physical parameters that are not necessarily independent of the time variable t. We suppose, on the other hand, that x_1 is the observed profile amplitude and that t can also represent the length of the profile (the profile length is proportional to t, because of a constant cutting speed). The attractor is then defined in the D-Volume, through the vector $(x_1(t),x_2(t),\ldots, x_D(t))$, which thus makes the study of the behavior of the system M easier. Nevertheless, two major difficulties relating to the manner of finding $x_2(t),\ldots$, and $x_D(t)$, as well as to that of the determination of the volume dimension of the phases space remain and will be overcome by recent techniques, concerning $x_2(t),\ldots$, and $x_D(t)$, and by an original method developed by the authors as regards the choice of D.

Remark. In order to facilitate the visualization of the attractor, with the maximum of information to allow the research of the characteristics of the signal dynamics, the method developed by the authors consists of a attractor projection, as defined by the delays vector of dimension D, in a space of size equal to its Euclidean dimension E ($D \geq E$). We obviously make sure that the projected scatter plot inertia $z(1)$, $z(2)$,..,et $z(N)$ defining a graph G is maximum. The Renyi dimensions built on G and determining a multi-fractal spectrum are thus identical to the attractor dimensions. This therefore means that the attractor fractal characteristics will remain unchanged, when the projected space dimension is identical to that of the attractor. Let us now note that each axis of the projections space is a linear combination of phase variables for the attractor. Let us note, on the other hand, that Fig. 14 is an illustration of the Henon attractor representation on the first two axes of the projection space. In the paragraphs that follow, our analysis process will be applied to simulated profiles, before considering the machined surfaces.

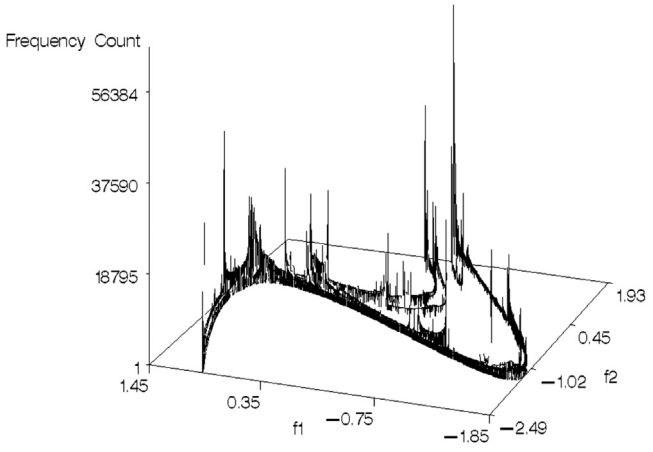

Fig. 14. Empirical density function of Henon's Attractor orthogonal projection on a two-dimensional plane.

4.3. Attractor characterization for the simulated surface profile

We choose a sinusoidal profile to illustrate our method. This choice seems appropriate for our analysis, since the profiles of machined surfaces we are studying possess an intrinsic periodicity. Indeed, both the calculation of delay vectors and the analysis of the graph $(y(n_i), y(n_i+1))$ representing the sinusoid attractor in

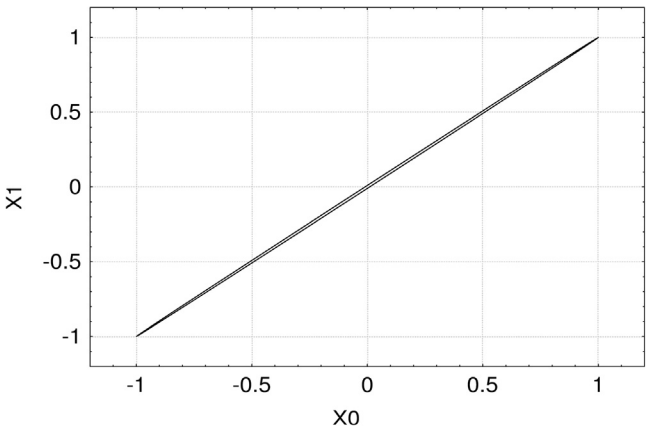

Fig. 15. Construction of the sinusoid attractor by the usual delay method.

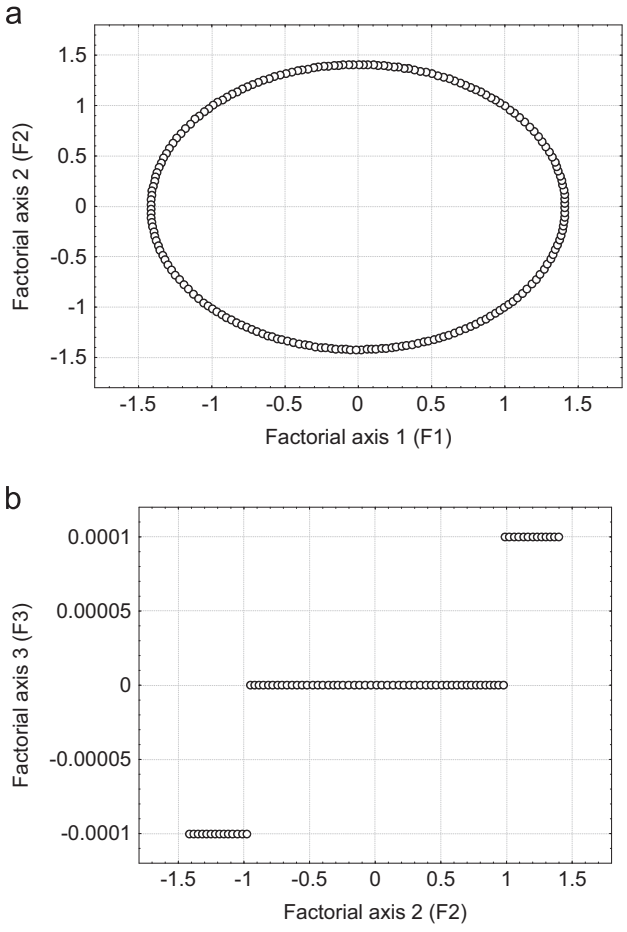

Fig. 16. Construction by our projection method of the sinusoid attractor on the two orthogonal axes F1–F2 (a) and the other axes F2–F3 (b).

dimension 2 (Fig. 15) show a strong linear correlation between the points $y(n_i)$ and $y(n_i+1)$, which considerably complicates a correct visualization. To avoid this difficulty the attractor is, at first, and according to our method, projected on the two-dimensional vector space (Fig. 16a) formed by the two first axes F_1 *and* F_2 of the projection space. We then obtain a circle, which finally proves the non-fractal aspect of the initial profile. Besides, by observing its projection on the space formed by the factorial second and third axes (Fig. 16b), the attractor appears as being almost reduced to a horizontal line parallel to axis 2, and then axis 3 seems to contain no relevant information. However, to better interpret these results, we chose to introduce the following fundamental theorem concerning the projection of the observed scatter diagram.

Theorem 1. *Let F_k be a subspace carrying the maximum inertia of a scatter diagram, then the subspace of dimension $k+1$ carrying the same maximum inertia is the direct sum of F_k with a subspace of dimension 1, orthogonal to F_k and carrying the maximum inertia too. The subspace F_k is thus built by successive estimates, or step by step, by seeking at first the subspace of dimension 1 of the maximum inertia, then a subspace of the same dimension 1, orthogonal to the precedent, and of maximum inertia, and so on.*

The analysis of the sinusoid attractor by means of this result gives the following interpretation: when the attractor is a circle, its fractal dimension is 1, and only two dimensions are enough to characterize it. To confirm this analysis, it is possible to rebuild the studied profile starting from each projection. Thus, Fig. 17a allows the rebuilding of the sinusoid starting from the first two axes of projection, whereas the third axis (Fig. 17b) does not almost contain any information, the trajectory amplitude being too low. The observed variations are primarily due only to a noise related to numerical calculations, and precisely due to the estimate of eigenvectors and eigenvalues necessary for projection.

4.4. Application of the analysis to a disturbed sinusoid

We initially start by analyzing an uncorrelated white noise which, naturally, is not easily analyzable by the chaos theory, but whose interest in the present study is to highlight a better comprehension of the noise which, a fortiori, sullies the experimental data.

4.4.1. Signature quantification of an uncorrelated white noise

For reasons of simplification, we consider a bounded noise between 0 and 1. However, a white noise is uncorrelated and then no relation occurs between $y(n_i)$ and $y(n_i+p)$ for $p \neq 0$, $\forall i$. Consequently, the attractor points are uniformly distributed in a square of dimensions $[0, 1] \times [0, 1]$, so that the attractor is identified with a plane of fractal dimension 2, for a sufficiently significant number of points. So, for a volume, that is when the attractor is built from coordinates $(y(n_i), y(n_i+1), y(n_i+2))$, it will be identified with a multitude of points uniformly distributed in the volume $[0,1]^3$ of fractal dimension 3. The same reasoning leads to a fractal dimension equal to n, for an attractor built in dimension n. Let now us proceed to the analysis of the white noise, when this last one is projected according to the method we implemented. The theorem that follows thus specifies the probability distribution shape of the projection of the delays vectors for a white noise.

Theorem 2. *Let $y(n_i)$ be the delays vector of dimension p, for a white noise, and let $P(y, p')$ be the operator of orthogonal projection that maximizes the projected scatter diagram on a space of dimension p', $(p' < p)$. Let $G(a, e_i, e_j)$ be the a-orthogonal projection on the plane defined by both basic vectors e_i and e_j, with $i \neq j \leq \dim a$, and let $\Psi_{i,j}(n, p, p')$ be the set of points defined by*

$$\Psi_{e_i,e_j}(n,p,p') = \{G(P(y_1(p,p')), e_i, e_j), G(P(y_2(p,p')), e_i, e_j), \ldots, G(P(y_n(p,p')), e_i, e_j)\} \quad (9)$$

Let $\Gamma(\Psi_{e_i,e_j}(n,p,p'))$ be the probability density of the distribution of points built on the basis of (e_i, e_j). If $y(p)$ is a random vector of uniform probability distribution between 0 and 1, then:

$$\lim_{\substack{n\to\infty \\ p\to\infty}} \Gamma\left(\Psi_{\substack{(x,0) \\ (0,y)}}(n,p,p')\right) = \frac{1}{4\pi} e^{-(x^2+y^2)/(4)} \quad (10)$$

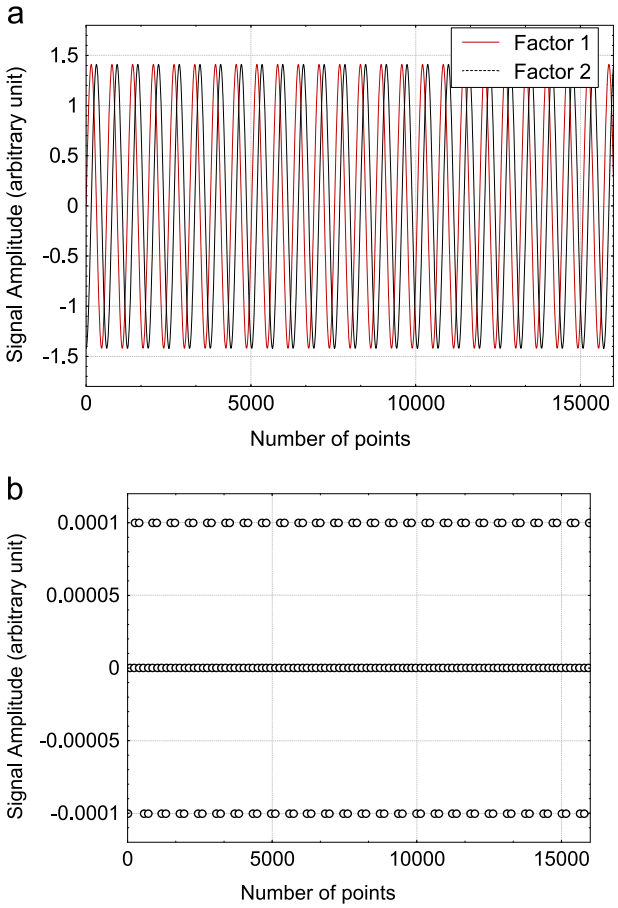

Fig. 17. Profile reconstruction of the sinusoid by the projection method on the two orthogonal axes F1 and F2 (a) and the other axis F3 (b).

Remark. The delay vectors are projected on a subspace of dimension 2. The histogram of such a projection is obtained by maximization of the inertia of the projected scatter diagram, and thus presents the shape of a two-dimensional Gaussian distribution, when the space dimension tends towards infinity. However, this theorem does not provide any indication on the convergence rate for the distribution of delays vectors, according to the projection subspace dimension. Nevertheless, Fig. 18 presents the probability density function of 50,000,000 delay vectors in 4-dimension on two subspaces.

4.4.2. Effect of the addition of a white noise on attractor rebuilding

For a studied system, the difficulty generally lies in the differentiation between the signal intrinsic noise (white noise) and the chaotic one which characterizes the nonlinear dynamics (pink noise). Besides, the infinity of dimensions which occupies a noise in the phases space complicates the determination of real dimension of the attractor. In order to illustrate this point, simulated profiles similar to the experimental ones (Fig. 19) are generated and a white noise is added with various amplitudes. The analysis of Fig. 20 represents the attractor projection on the first two axes according to the added noise amplitude. The following conclusions can be stated:

- The attractor tends towards a curve of fractal dimension 1 when the noise decreases. The signal thus becomes deterministic.
- No fundamental modification of the histogram shape is observed when the noise increases. This result proves the robustness of the original highlighted method for the attractor visualization. The analysis of the system dynamics properties which have generated the machined surface is therefore established.
- The dimension allowing an observation of the system dynamics, apart from the noise influence, is thus obtained. The attractor can, indeed, be perfectly characterized by the first two axes, i.e., in a subspace of dimension 2.
- The observed maximum of the probability density function does not depend on the noise intensity. It then characterizes the signal shape in the absence of noise.
- The profile dynamics is thus carried by the second axis, independent of the profile amplitude, as illustrated by the symmetry of the histogram with regard to a straight line passing by the second axis origin and parallel to the first one.

4.5. Application to the analysis of machined surfaces profiles

Experimentally, we have 30 surface measurements carried out in the same cutting conditions. Individual attractors are computed from each profile and all the points of these individual attractors are gathered to estimate global attractor probability density function. Fig. 21 represents these densities and their associated response surfaces for projection on a subspace of dimension 2 according to axes 1 and 2. Let us note that these last ones are obtained at various cutting speeds, and it results in the following remarks:

1. The projection of the initial attractor on the principal axes is carried out on a vector subspace whose eigenvectors, which actually are the basic vectors in the new coordinates system, are identical. On the other hand, a statistical analysis shows that the coordinates of the first axis vector in the former base (*the initial attractor base*) only depend very slightly on the cutting speed (Fig. 22.) We will thus admit for these coordinates, constant values:

$$x_0 = x_1 = 0.50015_{\pm 0.00025} \approx 0.5 \tag{11}$$

This means that the attractor point of coordinates (x'_0, x'_1) is projected on the first axis of the direction vector $(0.5x'_0, 0.5x'_1)$. Assuming that the chaotic mechanism is expressed in dimension 2, its equations can then be formulated as follows:

$$\partial x_0(t)/\partial t = \alpha_0 M_0(A_0, x'_0(t), x'_1(t)) + \alpha_1 M_1(A_1, x'_0(t), x'_1(t)) \tag{12}$$

Consequently, the first axis contains the two mechanisms M_0 and M_1 which model the dynamic system.
2. The modeling of disturbed machining led to forms of statistical distributions different from those represented by the histograms of Fig. 20; we deduce from it that the measured surface is not simply a perfectly machined surface on which a white noise is added.
3. When the cutting speed grows, the histogram changes from a unimodal distribution to a bimodal one. Both obtained modes are separated by a straight line perpendicular to the first axis and passing through the origin. This last one represents the gravity center projection for the initial attractor. Physically, this point represents an inertia center, i.e. a balance point for all points subset. Fig. 23 represents the scatter plot distribution which is projected on the first axis, according to the cutting speed. When the cutting speed is lower than 125 m/min, the attractor probability density is unimodal and involves for the dynamic system a convergence towards a fixed point that is the mode value. The system is thus not unstable and always turns over towards a balanced state whatever system disturbances are introduced by material heterogeneities and process variability. The stability of the dynamic system would thus result in the mechanisms M_0 and M_1 being closely bound, in the sense

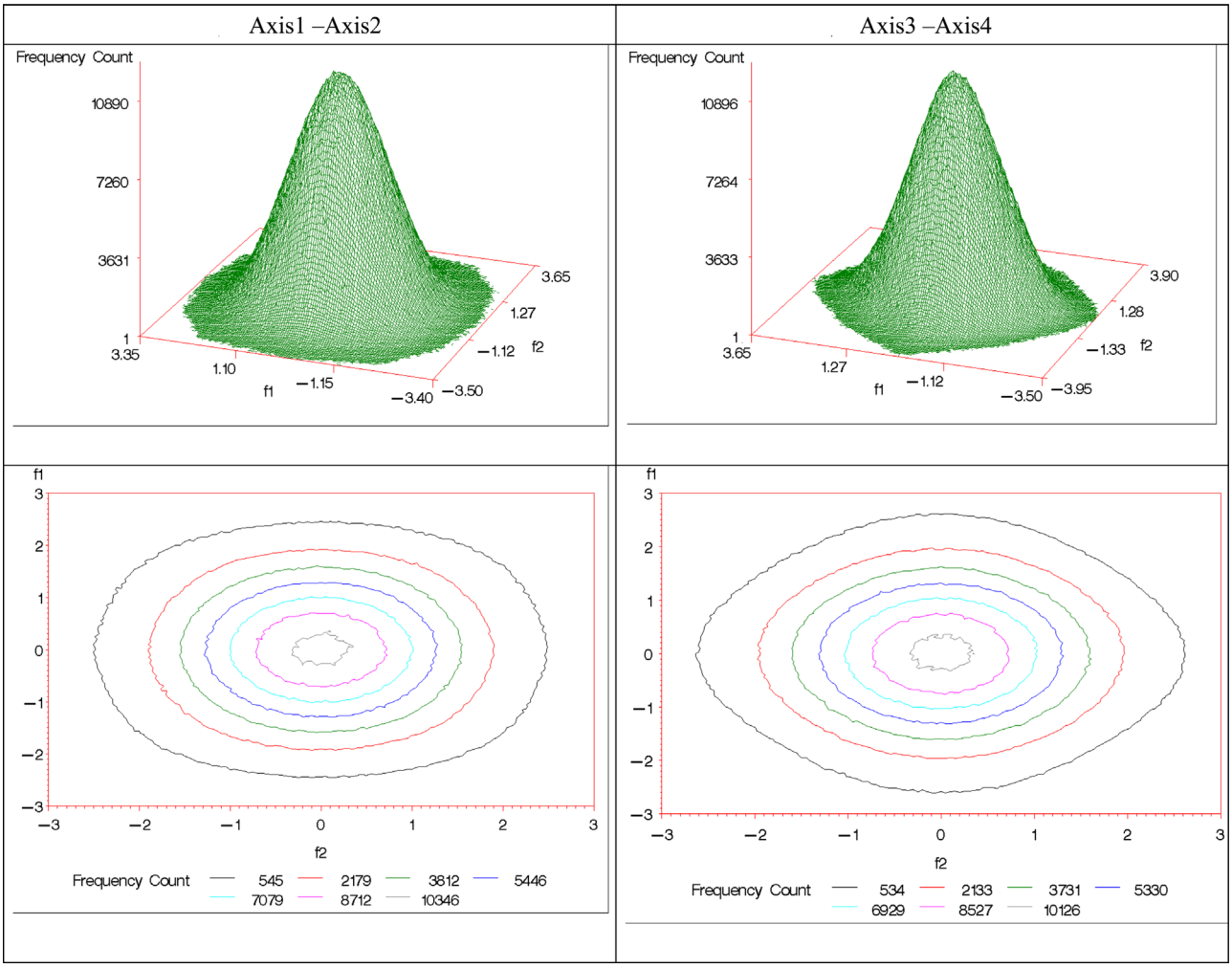

Fig. 18. Empirical density functions and their associated response surfaces of a white noise attractor by an orthogonal projection on a two dimensional plane defined by axes 1–2 and axes 3–4.

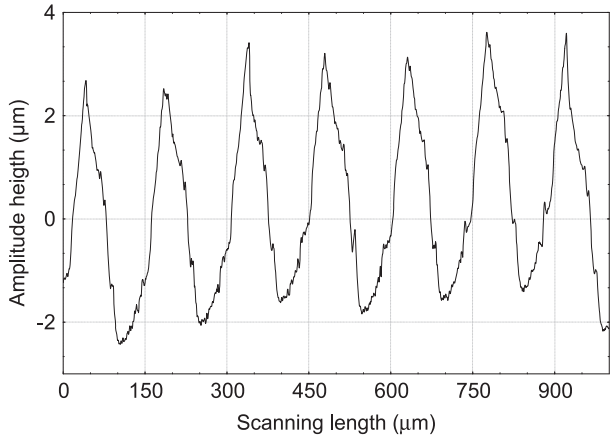

Fig. 19. Zoom of a roughness profile for a machined surface.

where none of them dominates the other during the cutting process. On the other hand, starting from a speed of 125 m/min, the attractor reaches a bifurcation and the system oscillates between two states $x'_a(t)$ and $x'_b(t)$. The alternation of the mechanisms M_0 and M_1 thus makes the system evolve from state A to state B, then A, then B, and so on. Consequently, one can admit the alternation of the two mechanisms M_0 and M_1 during the cutting process.

4.5.1. *Attractor characterization space dimension*

In what follows, we will try to establish that the mechanisms M_0 and M_1 are enough to describe the machinability dynamics. We will first start by examining the projection quality on each axis characterizing the attractor. By considering 10 axis, Fig. 24 reveals that nearly 99.9% of the scatter diagram inertia is carried by the first axis of projection that justifies all the analyses we have carried out on this axis. On the other hand, the observation of this same graph shows that the second axis is also carrying certain information, in spite of the small percentage of inertia which is due for it. In fact, this information is only subjective. One also notes, because of the shift observed between the mode, compared to the second axis, and for high cutting speeds, that this axis contains, contrary to axes 3 to 10, information on the dynamic processes M_0 and M_1. It thus appears, taking into consideration all these observations, that dimensions higher than 2 do not bring any information on machinability, which implies for the attractor a dimension equal to 2.

4.5.2. *Profiles rebuilding and analyses according to the axes*

Fig. 25, which represents a signal rebuilding according to the first four axes, allows the following remarks:

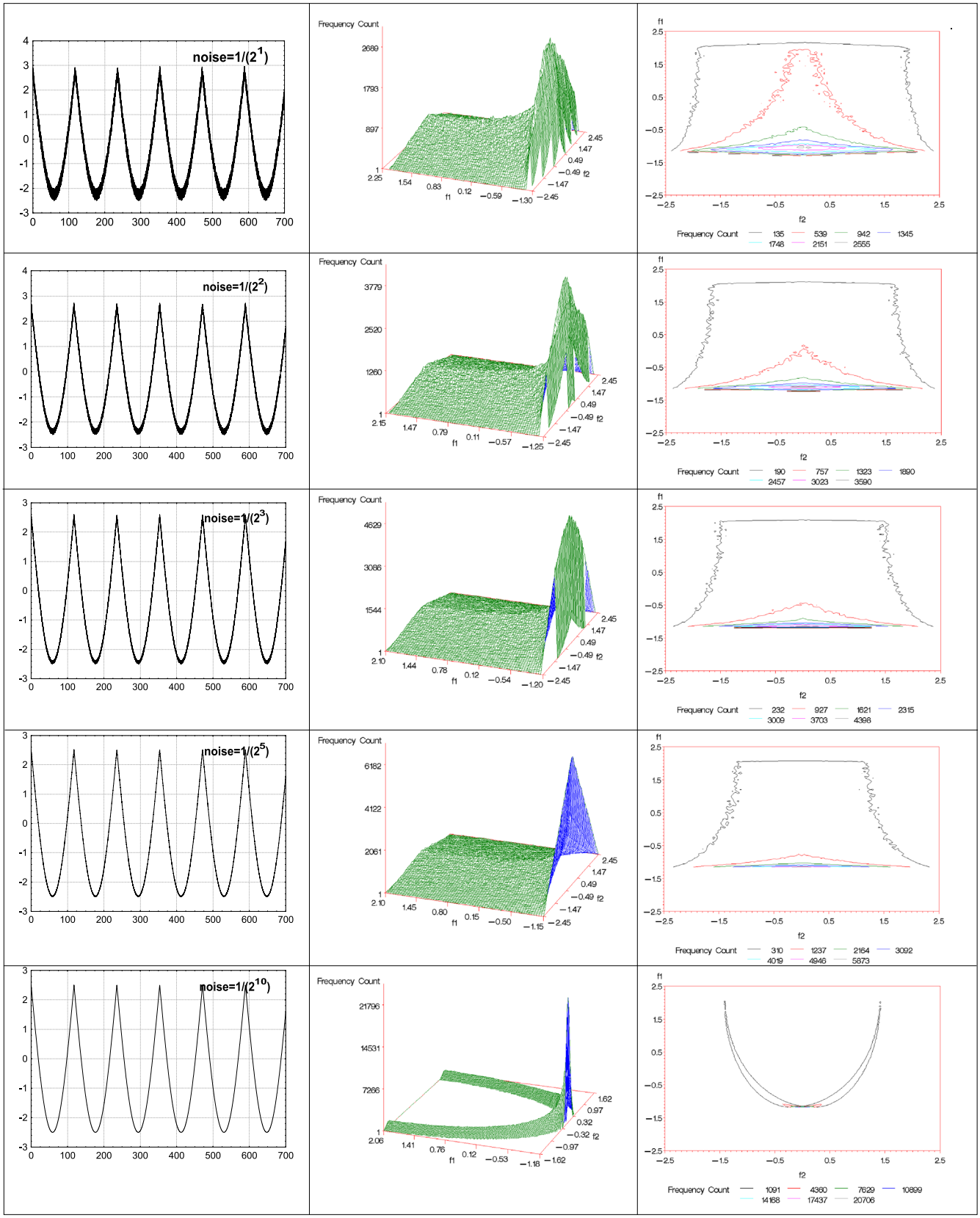

Fig. 20. Simulated profiles of the machined profile shown in Fig. 19 with an additional noise with different amplitudes, empirical density functions and the associated response surfaces of their attractor obtained by an orthogonal projection on a two-dimensional plane defined by the axes 1–2.

- Axes 3 and 4, the profiles can be identified as a white noise and obviously appear different from the first two axes.
- Whereas the first axis contains information on the macroscopic aspect of the machined profile, the second rather seems to contain on its micro-roughness (machining noise). In order to confirm this last assertion, the fractal dimension of the profiles projected, in particular on the first five axes, was calculated according to an original method [18]. Fig. 26 shows its evolution

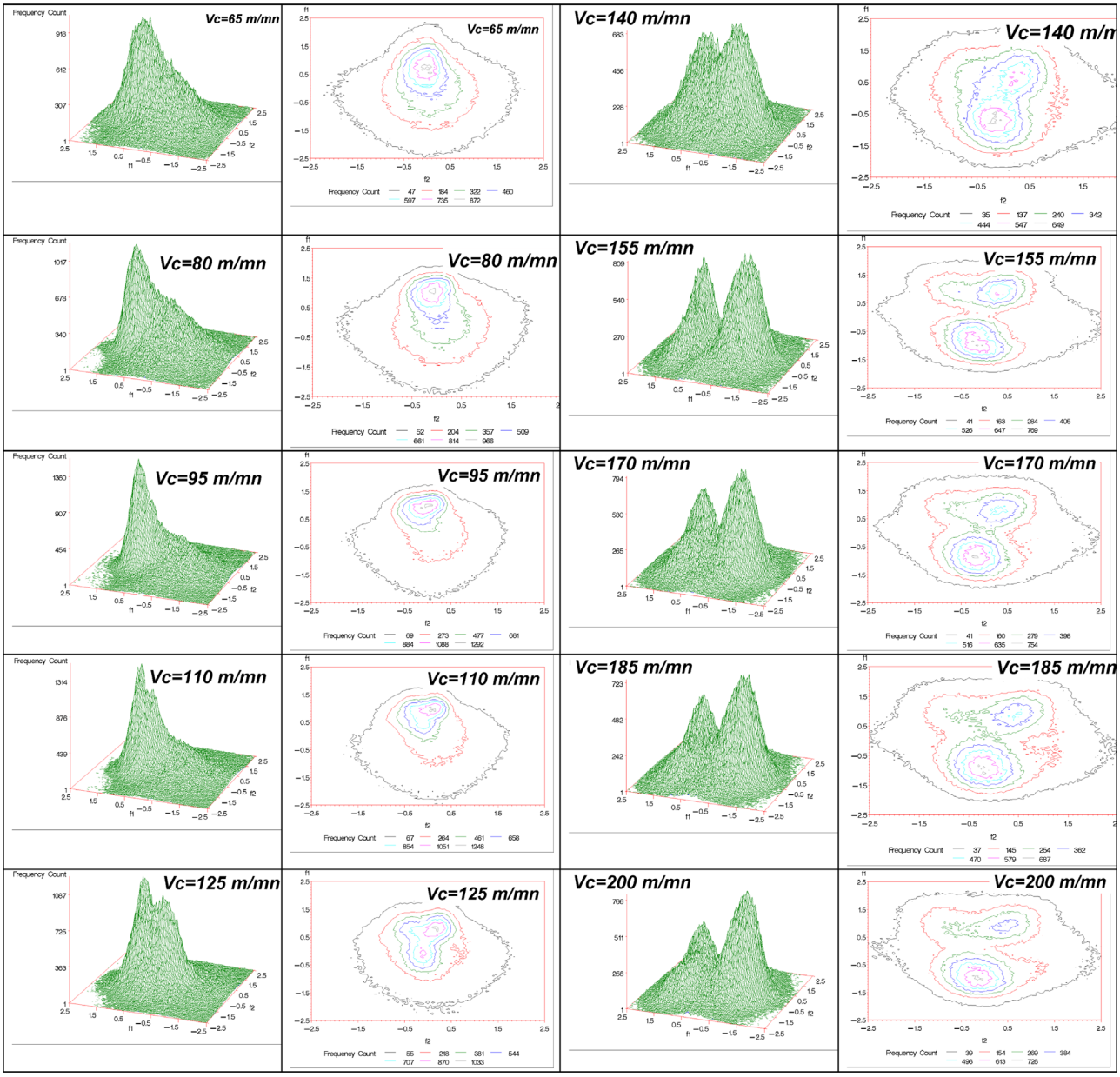

Fig. 21. Empirical density functions and associated response surfaces of attractor of experimental profiles with different cutting speeds (see Fig. 1) obtained by an orthogonal projection on a two-dimensional plane defined by the axes 1–2.

according to the cutting speed. It is followed from there, that the projection on axis 1 had the effect of regulating (smooth) the profile and leading to a fractal dimension close to 1, independent of the cutting speed. The highlighted method is thus robust and corresponds to an analysis of the profile carried out in the same Euclidean dimension whatever the machined profile shape. However, on the second axis, there is a fractal dimension ranging between 1.5 and 1.6. This value confirms that this axis contains information on the fractal nature (microscopic scale), excluding the presence of an uncorrelated noise. The existence of a common structure implies linear growth of the fractal dimension, according to the dynamic system oscillations, when the cutting speed increases. For lower speed, there is a fractal dimension of 1.5, meaning a long positive correlation length of the tool surfaces (diffusion or persistent state). For large cutting speeds, fractal dimensions reach 1.6, which involves a negative correlation length (sub-diffusive or antipersistance state). This clearly means that under the cutting speed of 125 m/mn the dynamical system is long and persistent and after this threshold it becomes anti-correlated, involving the succession of different states. The kinetics of the chaos generated by machining when the cutting speed increases is then carried by axis 2.

– Concerning axes 3, 4 and 5, the obtained fractal dimension tends towards 2 (fractal dimension of a white noise) without reaching this value (smoothing effect at small length due to tactile profilometer recording). This indicates the absence of relevant information on these axes.

Note: the methodology of projection that we developed thus made it possible to reveal only two dual scales for the machinability analysis of workability: one macroscopic and carried by the first axis, and the other microscopic and carried by the second. On the other hand, when the fractal dimension is calculated using the initial profiles (Fig. 27), it does not appear as a relevant parameter for characterizing the effect of cutting speed on machinability because measurements include simultaneously

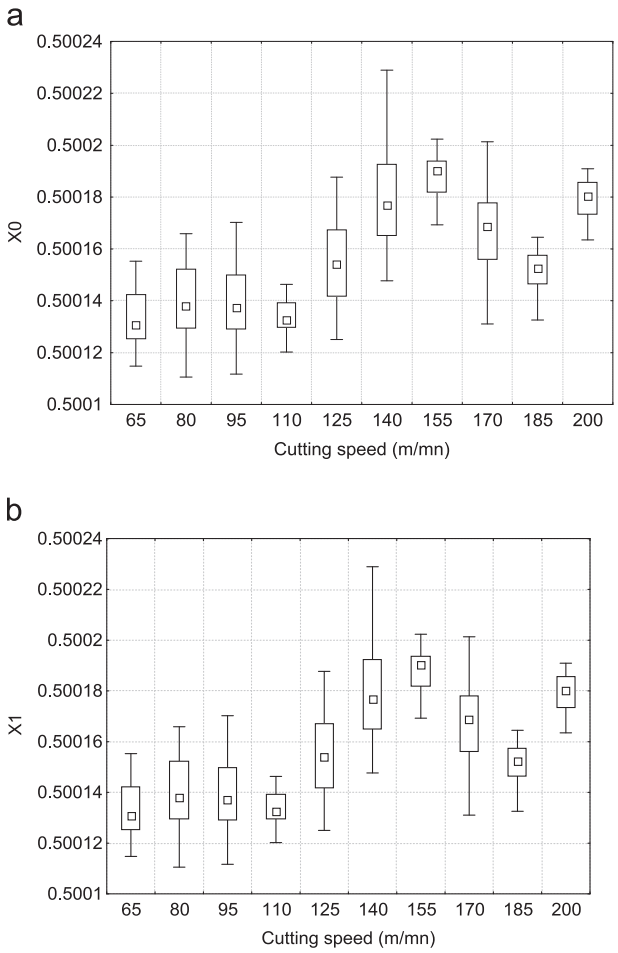

Fig. 22. Coefficient of the first dimension (a) and the second one (b) of the initial attractor projected on the first axis for different cutting speeds.

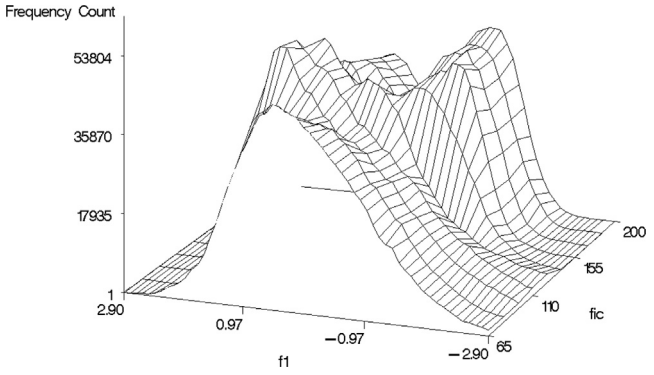

Fig. 23. Empirical density function and the associated surface response of Feigenbaum's plot of the reconstructed profile obtained by an orthogonal projection on a first axis versus the cutting speed.

macroscopic and microscopic roughness. Nevertheless, its measurement via our projection method allows its decomposition according to axes 1 and 2, and therefore highlights the cutting speed's influence on machinability carried by the second axis.

5. Results' interpretation of the machinability analysis via the chaos theory

We have clearly shown that the machinability was explained by two physical mechanisms that coincide at low speeds and alternate

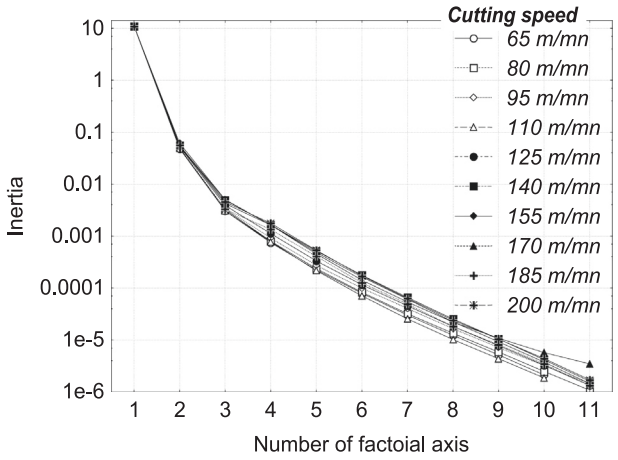

Fig. 24. Inertia of the projected attractor obtained at different cutting speeds versus the number of orthogonal axis.

at high cutting speed, generating an unstable chaotic behavior with two levels. This phenomenon can be explained in machining as follows: the process of cutting is governed by generalized strain hardening for low cutting speeds and by localized shear plastic deformation at high cutting speeds. In the latter case, the severity of plastic deformation and work-hardening at the surface region increase the yield stress near the surface. Indeed, the uniaxial traction constitutive relation is defined as follows:

$$\sigma = (A + B\varepsilon^n)(1 - CT)(1 + (\dot{\varepsilon}/D)^m) \tag{13}$$

where A, B, C, D, m, and n are material constants determined by quasi static, hot and dynamic compression, ε the true strain, $\dot{\varepsilon}$ the true strain rate and finally $\sigma/\sqrt{3} = \overline{\tau}$ represents the shear plastic deformation stress and $\gamma = \varepsilon\sqrt{3}$ the shear plastic deformation strain. The increase in cutting temperature in the shear plastic deformation plane is thus due to an increase in the shear plastic deformation stress, and thus to an increase in the corresponding strain when the cutting speed increases (*see Loewen and Shaw relation in* [8]):

$$T - T_\infty = \frac{0.9}{1 + 1.328\sqrt{K_I\gamma/V_c f}}\frac{\overline{\tau}\gamma}{\rho C_p} \tag{14}$$

where γ is shear strain, $\overline{\tau}$ is shear stress, C_p is heat capacity of the material, K_I is fracture toughness, T is cutting temperature, T_∞ is room temperature, V_c is cutting speed, f is feed rate and ρ is density of the material.

As the temperature yield stress increases, there appears a very large increase in temperature during cutting. This increase in temperature causes softening of the material, and consequently there is a shear plastic deformation stress reduction; it then follows a temperature reduction, with a return to the initial temperature. Consequently, a succession of cycles appears between the phases of hardening and softening. As regards the existence of the attractor fixed point, the explanation comes from the balance reached by the system. For sufficiently low cutting speeds (*the cutting process only occurring by generalized strain hardening*), the cutting process is an un-adiabatic process: since the heat has time to propagate through the material. The transition between the two highlighted mechanisms was analyzed by Recht [19]. This shows, as confirmed by our analysis, that the transition from the shear plastic deformation mode, which corresponds for this system to instability, occurs when the strain hardening effects are balanced by the thermal softening ones. The relation (15) then follows:

$$\frac{d\overline{\tau}}{d\gamma} = \frac{\partial\overline{\tau}}{\partial\gamma} + \frac{\partial\overline{\tau}}{\partial T}\frac{dT}{d\gamma} \tag{15}$$

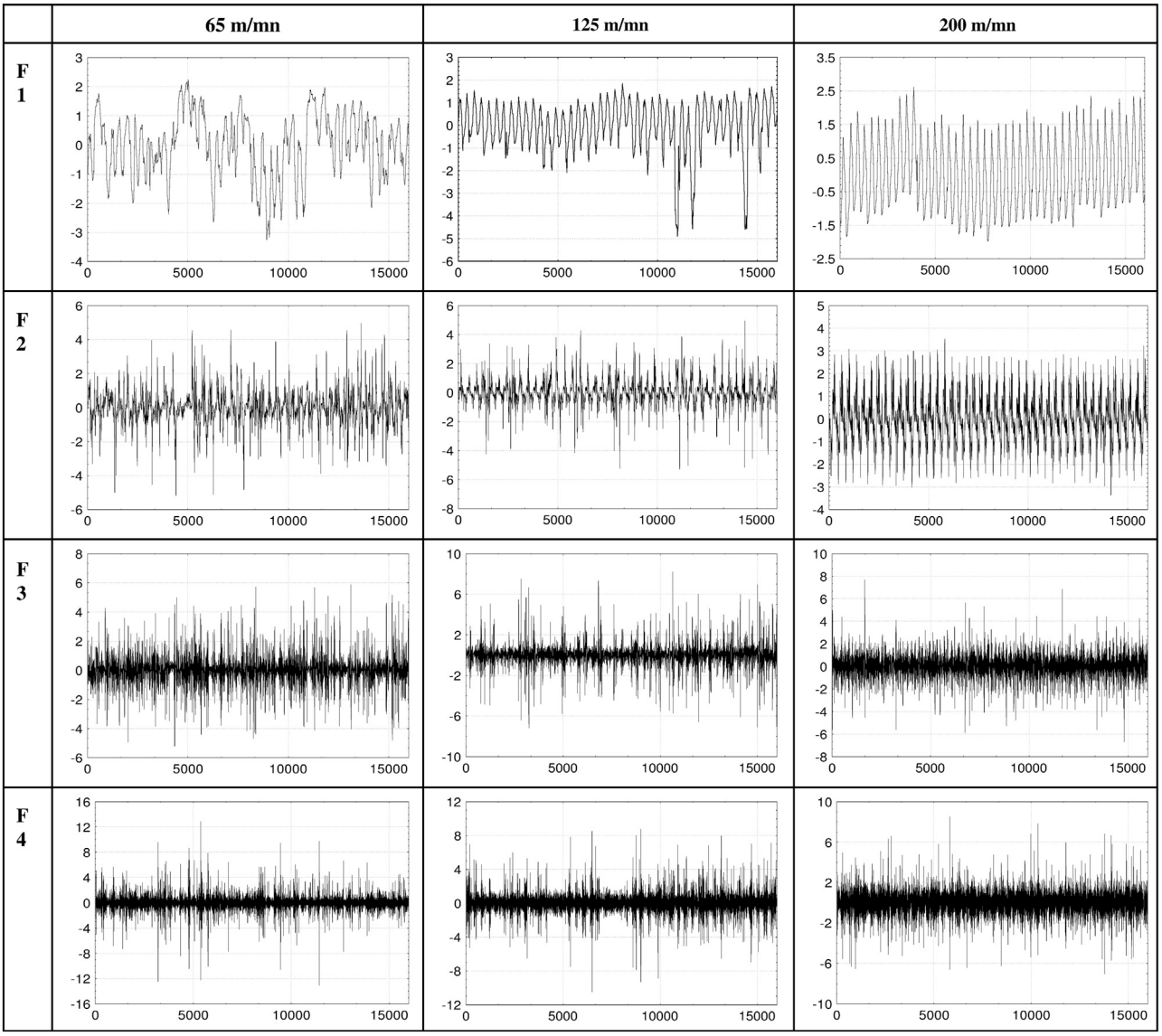

Fig. 25. Reconstruction of profiles of the attractor projected on axes 1–4 obtained at different cutting speeds.

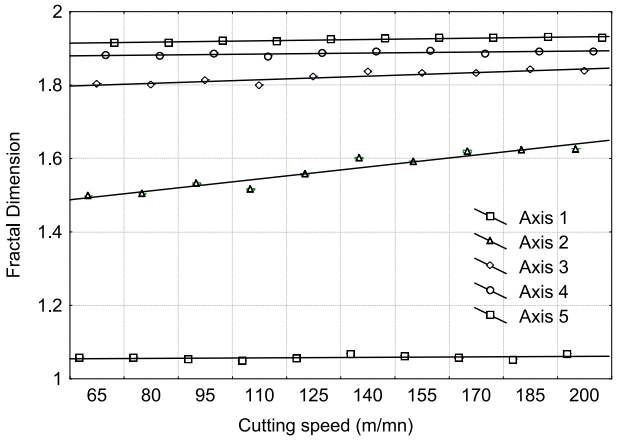

Fig. 26. Fractal dimension of the reconstructed profiles of the attractor projected on axes 1–5 (see Fig. 25) versus the cutting speed.

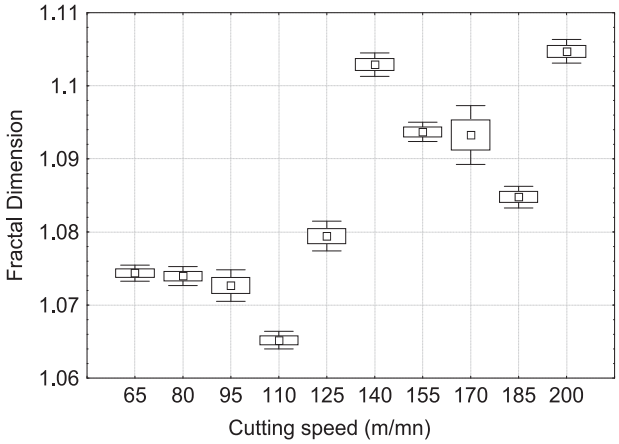

Fig. 27. Fractal dimension of profiles of the tooled surfaces (see Fig. 1) versus the cutting speed.

Recht thus established that strain hardening, which is the cause of cutting, can be expressed in the form of a linear combination of two differential mechanisms. In order to characterize the cutting speed influence on machinability, he then established the criterion based on the calculation of the term R defined as follows:

$$R = \frac{\partial \overline{\tau}/\partial \gamma}{(\partial \overline{\tau}/\partial T)(dT/d\gamma)} \quad (16)$$

a) If $R=1$ ($V_c=125$ m/min), there appears a transition mode, and the cutting speed is thus associated with the first bifurcation in Feigenbaum's diagram.
b) If $R<1$ ($V_c>125$ m/min), there appears a zone of localized shear plastic deformation, meaning the presence of chaotic mode with two states.
c) If $R>1$ ($V_c<125$ m/min), there appears a generalized shear plastic deformation zone, with an equilibrium state and fixed points in the attractor.

6. Conclusion

- Starting from roughness conventional parameters, we proposed in this work an original method for characterization of machinability, and then implemented a characterization method for analyzing the cutting speed influence on machinability, via the chaos theory.
- Regarding the conventional characterization of machinability, we highlighted the relevance of the average slope of the profiles, compared to a hundred other parameters, among which the parameter R_a is the most usually used. Indeed, the average slope of the profiles enabled us to differentiate two cutting modes, of which one is related to generalized strain hardening (*low cutting speed, high slopes of the profiles*), and the other is dependent on localized shear plastic deformation (*high cutting speed, weak slopes of the profiles*). The slope of profiles also allowed us, contrary to the parameter R_a, to quantify the cutting speed effect during each mode. The slope of profiles is relevant to easily determine in situ the effects of process parameters (*cutting speed, type of cutting machine, cutting depth, feed rate, etc*,) and to increase surface integrities (*internal stresses reduction, shape defects minimization, cutting power decreasing, increase in lifetime of the cutting machine, etc.*).
- From the chaos theory, it appears that the transition (generalized strain hardening / localized strain hardening) corresponds to a bifurcation on a Feigenbaum diagram built from roughness profiles. The highlighted original technique of projection allows us to establish that the two dimensions of the attractor characterize the two physical mechanisms, namely strain hardening of material and heat transfer during cutting operation. The apparition of a two chaotic mode highlights the balance between the strain hardening and the generalized shear plastic deformation that governs the transition mode in cutting process (adiabatic cutting). Let us note, on the other hand, that any calculation on the attractor itself (*multifractal spectrum, Lyapunov exponent*, etc.) was voluntarily excluded from this study to provide to the machinist during the adjustment of cutting conditions a simple graphic interpretation (the attractor plot).
In future works, we will measure roughness in the machining direction to confirm our analyses. It is proposed to extend this study to high-speed machining, in order to search for other bifurcations (Feigenbaum constant estimation). Finally, an analytical formulation of the attractor characteristics, through functions related to the hardening and the thermal effect, will be proposed in relation to morphological and microstructural study of the chips.

References

[1] Bigerelle M, Najjar D, Iost A. Description d'une nouvelle méthode de corrélation entre la rugosité et une propriété de surface, application à la brillance de tôles skin-passées, Revue de Métallurgie; Mai 2002. p. 467–79.
[2] Bigerelle M, Najjar D, Iost A. Relevance of roughness parameters for description and modelling of machined surfaces. J Mater Sci 2003;38(11):2525–36.
[3] Efron B. Bootstrap methods: another look at the jacknife. Ann Statis 1979;7:1–26.
[4] Efron B, Tibshirani RJ. An introduction to the bootstrap. London: Chapman and Hall; 1993.
[8] Poulachon G, Moisan AL, Dessoly M. Contribution à l'étude des mécanismes de coupe en tournage dur. Méc Ind 2002;3:291–9.
[9] Brewer J, Di Girolamo L. Limitations of fractal dimension estimation algorithms with implications for cloud studies. Atmos Res 2006;82(1–2):433–54.
[10] Charkaluk E, Bigerelle M, Iost A. Fractals and fracture. Eng Fract Mech 1998;61:119–39.
[11] Karube S, Hoshino W, Soutone T, Sato. K. The non-linear phenomena in vibration cutting system. The establishment of dynamic model. Int J Nonlinear Mech 2002;37:541–64.
[12] Gans RF. when is cutting chaotic? J Sound Vib 1995;188:75–83.
[13] Fofana MS. Sufficient condition for the stability of single and multiple regenerative chatter. Chaos, Solitons Fractals 2002;14:335–47.
[14] Fofana MS. Effect of regenerative process on the sample stability of a multiple delay differential equation. Chaos, Solitons Fractals 2002;14:301–9.
[15] Peitgen HO, Jürgens H, Saupe D. Chaos and fractals: new frontiers of science. New York: Springer-Verlag; 1992.
[16] Ruelle D. Chaotic evolution and strange attractor. Accademia Nazionale Dei Lincei : Cambridge University Press; 1987.
[17] Takens F. Detecting strange attractors in turbulence, Dynamical systems and turbulence, lectures notes in mathematics, vol. 898. New York: Spinger; 1981.
[18] Bigerelle M, Iost A. Calcul de la dimension fractale d'un profil par la méthode des autocorrélations moyennées normées A.M.N. C R Acad Sci 1996;t323(Série IIb):669–75.
[19] Recht FF. Catastrophic thermoplastic shear. J Appl Phys 1964;31:189–93.